Cortical neural activity predicts sensory acuity under optogenetic manipulation.

John J. Briguglio[1,3], Mark Aizenberg [2], Vijay Balasubramanian [1], Maria N. Geffen [2]*

1. Department of Physics, University of Pennsylvania, Philadelphia, PA
2. Department of Otorhinolaryngology: HNS, Department of Neuroscience, University of Pennsylvania, Philadelphia, PA,
3. Janelia Research Campus, Ashburn, VA

**Corresponding author:* Maria N. Geffen
Email: mgeffen@med.upenn.edu

Abstract.

Excitatory and inhibitory neurons in the mammalian sensory cortex form interconnected circuits that control cortical stimulus selectivity and sensory acuity. Theoretical studies have predicted that suppression of inhibition in such excitatory-inhibitory networks can lead to either an increase or, paradoxically, a decrease in excitatory neuronal firing, with consequent effects on stimulus selectivity. We tested whether modulation of inhibition or excitation in the auditory cortex could evoke such a variety of effects in tone-evoked responses and in behavioral frequency discrimination acuity. We found that, indeed, the effects of optogenetic manipulation on stimulus selectivity and behavior varied in both magnitude and sign across subjects, possibly reflecting differences in circuitry or expression of optogenetic factors. Changes in neural population responses consistently predicted behavioral changes for individuals separately, including improvement and impairment in acuity. This correlation between cortical and behavioral change demonstrates that, despite complex and varied effects these manipulations can have on neuronal dynamics, the resulting changes in cortical activity account for accompanying changes in behavioral acuity.

Author summary.

Excitatory and inhibitory interactions determine stimulus specificity and tuning in sensory cortex, thereby controlling perceptual discrimination acuity. Modeling of such excitatory-inhibitory circuits has predicted that suppressing the activity of inhibitory neurons can lead to increases or, paradoxically, decreases in excitatory activity, depending on the architecture and modulation parameters of the inhibitory component of the network. Here, we capitalized on differences between subjects to test whether suppressing/activating inhibition and excitation across a range of parameters in sensory cortex can in fact exhibit such paradoxical effects for both stimulus sensitivity and behavioral discriminability. Indeed, we found that the same optogenetic manipulation in the auditory cortices of different mice could improve or impair frequency discrimination acuity, in a fashion that was predictable from the effects on cortical responses to tones. The same manipulations sometimes produced opposite changes in the behavior of different individuals, supporting theoretical predictions for inhibition-stabilized networks.

Introduction.

Sensitivity to sensory signals depends on neuronal tuning to specific parameters of sensory stimuli, such as orientation of edges for visual stimuli, or tone frequency for auditory stimuli. Such neuronal selectivity arises in many brain areas and is shaped by complex, interconnected circuits of excitatory and inhibitory neurons [1]. The balance between inhibitory and excitatory stimulus representation in the sensory cortex has been proposed to underlie learning- and adaptation- dependent changes in stimulus-driven responses [2]. Recently, a number of studies have begun to unravel the role of inhibition in sensory processing, empowered by recently developed optogenetic techniques [for example 3, 4-10]. These methods drive specific classes of neurons to express an opsin, such that shining light over that brain area either activates or suppresses neuronal activity selectively [11-15].

While optogenetic techniques provide exquisite molecular and temporal specificity for testing the function of specific cell types in sensory acuity, they currently carry inherent and technical limitations that can lead to different levels of opsin expression and activation or suppression strength across individual animals. Since measurements are typically performed in multiple animals, these specific differences are accounted for using statistical analyses while summarizing the average effects of optogenetic perturbations. We postulated that these differences could be instead *exploited* in order to characterize the diversity of effects across subjects, thereby deepening our understanding of the function of inhibitory-excitatory interactions in sensory processing.

Theoretically, it has been predicted that within balanced excitatory-inhibitory circuits, increasing inhibition can either decrease excitatory neuronal activity or, paradoxically, increase it, depending on specific perturbation parameters and circuit properties [16]. We therefore hypothesized that the differences in technical parameters of optogenetic stimulations across animals could evoke both positive and negative effects on the firing rate of the target neuronal population. Focusing on tone frequency representation in the auditory cortex [9], we tested whether this was indeed the case by up- or down- regulating the activity of either inhibitory or excitatory neurons and measuring the resulting changes in frequency discriminability based on neuronal population activity. Our previous analyses had demonstrated that, on average, suppressing the activity of the most common class of interneuron, parvalbumin-positive neurons (PVs), in auditory cortex (AC) impaired behavioral frequency discrimination acuity, while activating PVs improved it, whereas activating excitatory neurons did not have an effect [9]. Here,

83 we compared changes in neuronally predicted and behavioral frequency discrimination acuity due
84 to optogenetic manipulations.

85 Optogenetic interventions led to changes in tone-evoked responses of recorded neurons. As
86 predicted, the same manipulation sometimes produced opposite changes in neurometric
87 sensitivity and in behavior for different individuals. Computational analysis predicted consequent
88 changes in discrimination thresholds, which explained the measured behavioral changes,
89 including improvement or impairment of discrimination driven by the same optogenetic
90 manipulation in different individuals. Our results thus demonstrate that, although these
91 manipulations have complex effects on the neural network, the resultant changes in activity are
92 sufficient to predict changes in behavior.

93 Results.

94 Measuring frequency discrimination acuity.

95 To measure frequency discrimination acuity, we used a procedure based on pre-pulse
96 inhibition of the acoustic startle reflex (Figure 1A, B). Like other mammals, mice startle to loud
97 noise. The startle response, as measured by the change in pressure exerted by the subject on a
98 balance platform, is typically decreased when the startle noise is preceded by a brief tone that
99 mice can detect – a phenomenon termed pre-pulse inhibition (PPI). We presented mice with a
100 continuous tone at one frequency, which was stepped to a tone of a different frequency just prior
101 to the startle noise. The startle response was attenuated as the frequency difference between
102 background and pre-pulse tones increased (Figure 1B, C). This attenuation reflects the ability of
103 the mouse to detect frequency differences [9, 17]. We characterized frequency discrimination
104 acuity in terms of a *behavioral threshold* -- the frequency difference that produced 50% of the
105 maximum PPI (Figure 1 C).

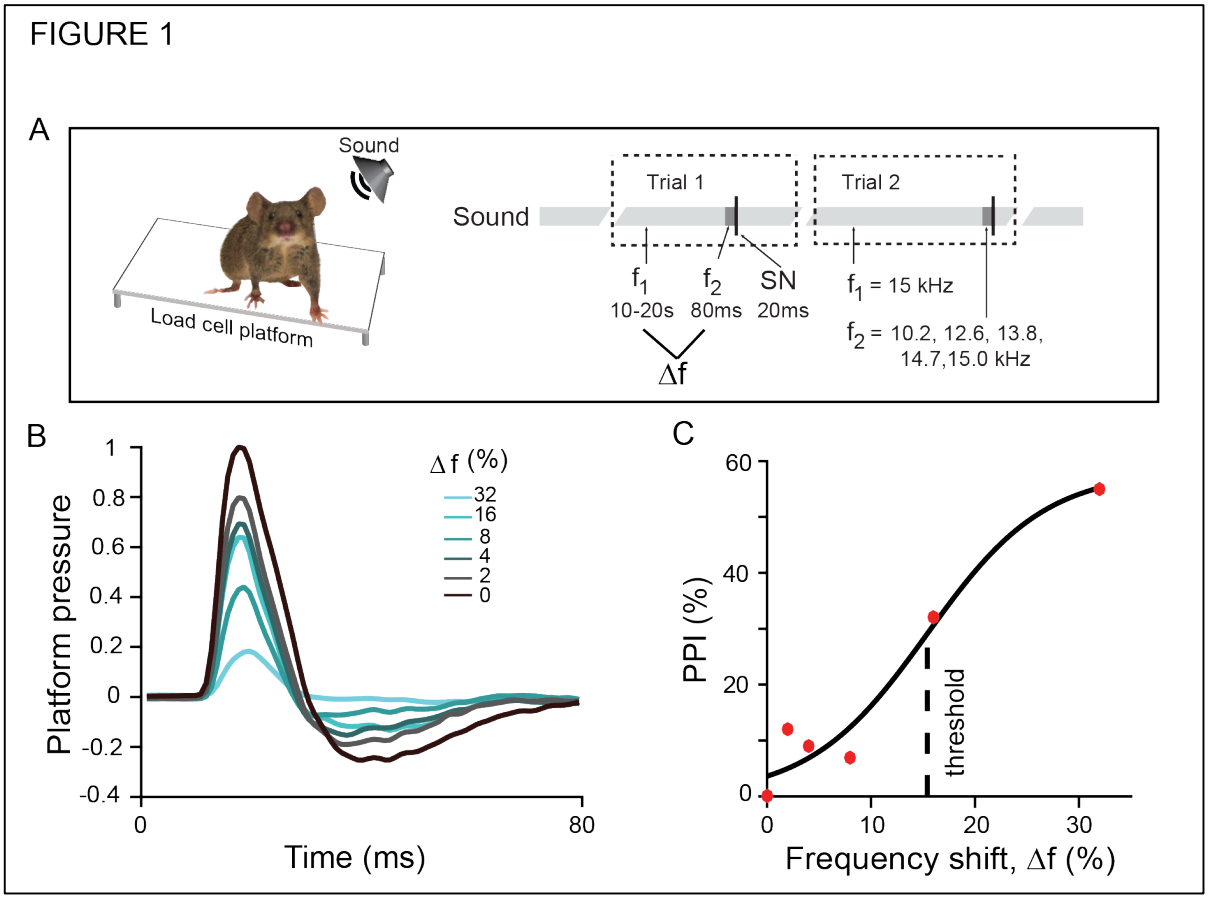

Figure 1: Measurement of behavioral frequency discrimination acuity.
A. Schematic of measurement of frequency discrimination acuity in mouse. **Left**: Startle response is measured as pressure the subject exerts on a platform. **Right**: Sound stimulus time course: an ongoing background tone (light gray, f_1) is followed by a brief pre-pulse tone of different frequency (dark grey band, f_2,) and then by a startle noise (thin black band, SN).
B. Normalized time course of platform pressure during the startle response to noise for different pre-pulse tones for an exemplar mouse. Time relative to SN onset.
C. Pre-pulse inhibition measured as reduction in the acoustic startle response as a function of the frequency shift (Δf) between the background and pre-pulse tones (see Methods for definition) of an exemplar mouse. PPI does not reach 100% because even with an easily identifiable prepulse tones, the animal still startles. Dots: data, solid line: fit.

Neurometric discrimination thresholds from Fisher Information

Next, we recorded the activity of putative excitatory cells (Methods) in AC, while presenting the awake head-fixed mouse with a random tone pip stimulus (50 ms tone pips presented every 500 ms, frequency changed at random, Figure 2A). For each frequency-tuned neuron, we measured frequency response curves (mean firing rate as a function of tone frequency, Methods and Figure 2B). To estimate a discrimination threshold from the frequency-tuned neural population recorded in each mouse we used Fisher Information analysis. To do so, we fit Gaussian functions to the response curve of each neuron, and assumed that neurons responded

independently and with Poisson variability. Standard methods then provided the Fisher information for frequency discrimination based on the population response (Methods; Figure 2C) [18]. Fisher information quantifies the amount of information that neural responses provide to distinguish nearby frequencies. Decoding sensitivity increases with Fisher information. Since this information is large when the neural response changes quickly as a function of frequency, it is higher on the slopes of the tuning curves than in the center.

The inverse square root of the Fisher Information bounds the accuracy with which nearby frequencies can be distinguished based on population activity. This quantity is by definition the *neurometric threshold*, and gives the frequency difference that can be discriminated with 70% accuracy. Figure 2D shows the neurometric thresholds determined in an individual mouse on the basis of the neural population recorded in its cortex.

A direct comparison of the neurometric threshold with behavior faces three challenges: (a) discrimination accuracy need not translate linearly into thresholds determined from the pre-pulse inhibition of the acoustic startle response measured here, (b) cortical recordings inevitably sub-sample the population of responsive neurons, and (c) frequency discrimination is supported by multiple pathways, some of which may not involve the auditory cortex. In general, we expect the neurometric thresholds computed here to be higher than the behavioral thresholds, because of the limited number of recorded neurons (e.g., Figure 2D).

In view of these challenges we did not seek to predict absolute behavioral thresholds from the population of recorded frequency-tuned neurons. Rather, we made a differential estimate: we manipulated excitatory and inhibitory neuronal activity in the auditory cortex optogenetically, and tested whether there was a correlation between the resulting *changes* in the neurometric estimate of discrimination thresholds and corresponding changes in behavior.

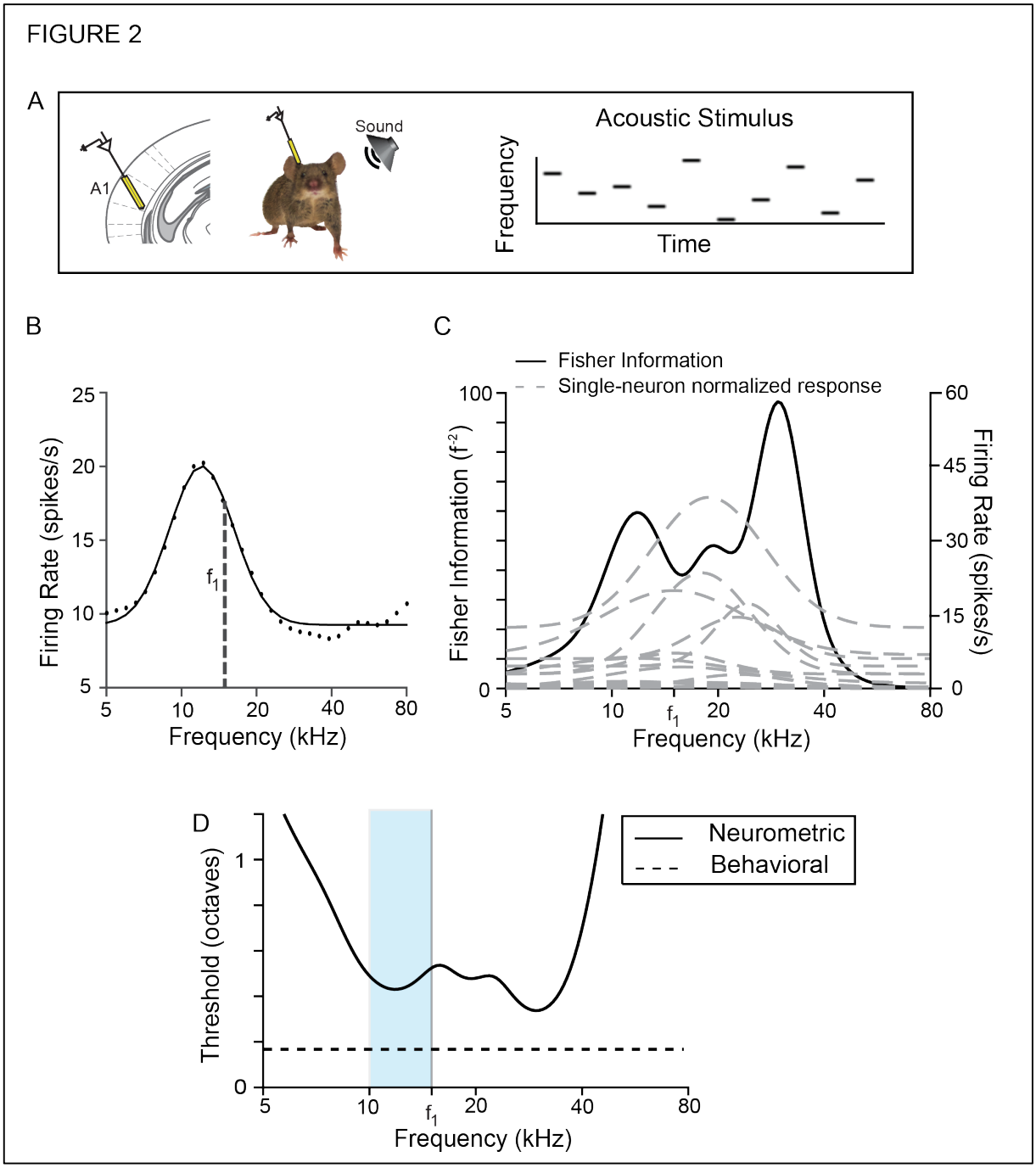

Figure 2: Measurement of neurometric frequency discrimination acuity.

A. **Left**: Schematic of electrophysiological recording of neuronal responses in the primary auditory cortex (A1) in awake mouse. **Right**: The stimulus consists of a pseudorandom sequence of pure tones at varying frequency and intensity levels.

B. Representative frequency response function for a single neuron (f_1 = background tone in Fig. 1). Black dots: data, black line: fit.

C. Fisher information for tone discrimination (black) computed on the basis of frequency response functions (gray dashed) of neurons (N=14) recorded in the same mouse.

D. Neurometric threshold for decoding frequency (solid) computed on the basis of the inverse square root of Fisher Information computed in **C**. The neurometric threshold based on the recorded population lies above behavioral threshold for discrimination around f_1 (dashed line). Light blue band indicates the region in frequency space from which behavioral measurements were taken.

166

167 ## Optogenetically induced changes in neurometric and behavioral thresholds are correlated.

168 Frequency tuning of AC neurons is thought to depend on the combination of excitatory and
169 inhibitory inputs [9, 19-22]. To manipulate tone responses of AC neurons, we targeted the most
170 common interneuron subtype, parvalbumin-positive interneurons (PVs). We drove PVs to express
171 Archaerhodopsin (Arch) or Channelrhodopsin (ChR2) by injecting a floxed Arch- or ChR2-
172 encoding virus in PV-Cre mice. We verified the efficiency of the viral transfection and light
173 stimulation by measuring the effect of light on spontaneous firing rates of neurons. As expected,
174 when PVs were activated by light, thus increasing inhibition, spontaneous activity decreased in
175 the recorded population (Figure 3A) [10]. Optogenetically suppressing PVs had the opposite
176 effect: the spontaneous rate of most recorded neurons increased (Figure 3B). We also drove
177 excitatory neurons in AC to express ChR2 and found that optogenetic illumination of AC led to an
178 elevated spontaneous firing rate (Figure 3C). Thus, we reliably used light to manipulate the
179 activity of excitatory and PV neurons in AC.

180 We next measured the behavioral effects of manipulating neural activity in AC. On half of the
181 trials, we illuminated AC at the same time as providing the pre-pulse stimulus. Activating PVs
182 (Figure 3D) decreased the threshold for most animals (N=5) and increased it for some (N=2),
183 while a few (N=4) did not have a statistically significant threshold change. Suppressing PVs
184 (Figure 3E) produced an increase in the frequency discrimination threshold for two animals, and
185 did not produce statistically significant change for one animal. Optogenetically activating
186 excitatory neurons increased the threshold for most animals (N=3) and decreased it for one, with
187 one animal displaying no threshold change (Figure 3F). For several animals, (N=6) the
188 manipulations did not produce any significant behavioral changes.

189 Finally, we measured the effect of manipulating neuronal activity on the neurometric frequency
190 discrimination thresholds predicted from the recorded population. Activating PVs led to a
191 decrease in the predicted threshold (Figures 3G, 4A, B, blue) for most PV-ChR2 mice (N=7) and
192 an increase for some (N=2). The predicted threshold increased for three PV-Arch mice after
193 suppressing PVs (Figures 3H, 4A, B green), but decreased for two. Activating excitatory neurons
194 (Figures 3I, 4A, B, red) increased the predicted threshold for all CamKIIa-ChR2 mice (N=3).
195 There was no predicted change for two mice (<2% change in predicted threshold).

196 A potential confound for optogenetic manipulation of cortical activity is the scattering of light
197 through the tip of the optic fiber. To prevent the light manipulation to serve as an additional pre-
198 pulse, we placed a bright LED in the chamber, which served to adapt the retina of the mouse to
199 scattered light from the optic fiber [23]. Another limitation of light-driven manipulations of neuronal

activity is a potential cascade of prolonged circuit-level dynamics. Therefore, to facilitate the comparison of the effect on light-off and light-on trials, light was presented on light-off trials as well, but not concurrent with the prepulse and startle stimuli. Indeed, light presentation alone did not affect the startle response (PV-ChR2 mice, blue light: N = 11, $p>0.05$; PV-Arch mice, green light: N = 8, $p>0.05$) and thus did not serve as a pre-pulse of the acoustic startle response. As an additional control, we injected a cohort of mice with virus carrying only the fluorescent reporter, and not the opsin. In these animals, there were no significant effects on frequency discrimination acuity (N = 6, $p>0.05$) [9]. These two aspects of stimulus design and control measurements thus confirmed that the observed behavioral changes were unlikely due to artifacts of light presentation, but rather due to light-driven manipulation of cortical activity.

For most individuals (N=15/19) and on average, the sign of the neurometric change in threshold with the optogenetic manipulations matched the sign of the change in behavioral threshold (Figure 4A, B). This qualitative agreement was striking, given that the electrophysiological recordings only sample a few neurons, while the light has a global effect on the auditory cortex and sometimes leads to opposite behavioral changes. To quantify the correlation, we compared the neurometric and behavioral frequency discrimination thresholds for each mouse, under light-on and light-off conditions. The number of recorded tone-responsive neurons varied significantly between mice (14-104 per animal). Using the linear dependence of the Fisher Information on population size we estimated that ~1000 independent neurons would be necessary for the neurometric thresholds to match the absolute behavioral thresholds (see Methods). This number differed between different mice, presumably because of the limited sampling, although was consistent in order of magnitude. Since optimizing the size of the population for each mouse would have skewed analysis across subjects, we divided the Fisher Information computed from the population by the number of neurons, and then scaled the result back linearly to the same effective population size for all mice (N = 1000 units).

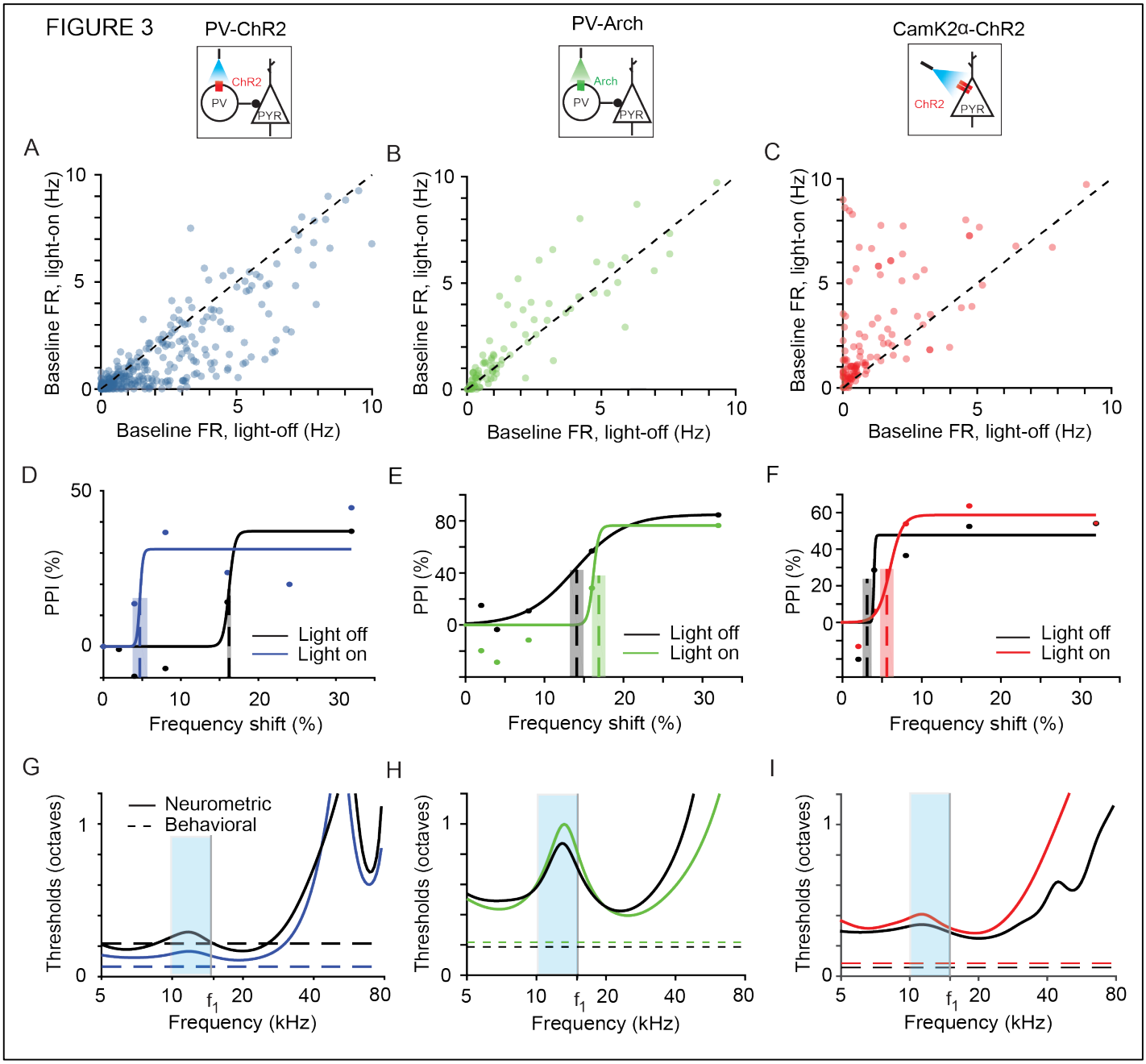

Figure 3: Optogenetic manipulation of PV activity shifts behavioral and neurometric frequency discrimination thresholds in individual subjects.

A,B,C: Baseline firing rate of light-on versus light-off trials for all frequency-tuned neurons pooled across subjects in PV-ChR2 (Blue), PV-Arch (Green), CamK2a-ChR2 (Red) mice, respectively. **D,E,F**: PPI as a function of tone frequency shift for exemplar mice. Best estimated thresholds (dashed lines) and uncertainties (overlaid gray rectangle) are plotted for reference. Black: light-off trials; Blue, Green, Red: light-on trials. Dots: data, solid lines: best fit curve. **G,H,I**: Neurometric threshold estimate as inverse square root of Fisher information (solid) and behavioral threshold at f_1, (horizontal dotted) for the same mice as **D,E,F**. Light blue bands indicate the region in frequency space from which behavioral measurements were taken.

We next compared the resulting estimate to the behavioral threshold. We first found a correlation between the absolute behavioral and neurometric thresholds under all conditions (Figure 4A, S2 Figure, S1 Table). The correlation was statistically significant ($C = .37$, $p = .02$, $N = 38$, including a light-on and a light-off measurement for each of 19 mice), but only weakly so. To test more closely the effect of the optogenetic manipulations, we computed an index of change as the difference in thresholds before and after application of light, divided by the sum. We found that index of change of the neurometric thresholds was strongly correlated with the behaviorally measured index of change in frequency discrimination acuity threshold (Figure 4B, $C = .59$, $p = .007$, $N = 19$).

These correlations suggest that: (a) auditory cortex does modulate frequency discrimination behavior, (b) the effects seen in the small recorded patch are representative, and (c) individual differences in auditory behavior are directly driven by differences in excitatory and inhibitory interactions in cortical circuits.

		Behavior						Neurometric (scaled)			
Mouse	Type	T_{off} (%)	ΔT_{off} (%)	T_{on} (%)	ΔT_{on} (%)	I_{change}	ΔI_{change}	T_{off} (%)	T_{on} (%)	I_{change}	Neurons
1	PV-Arch	21.5	1.7	22	2	0.00	.06	6.4	9.1	.17	42
2	PV-ChR2	16.2	.3	4.7	.1	-.53	.07	7.9	4.7	-.25	104
3	PV-ChR2	22	4	6.0	1.7	-.54	.11	8.7	6.5	-.14	16
4	PV-ChR2	13.7	1.5	4	3	-.54	.3	22.8	10.6	-.34	20
5	PV-ChR2	16.7	1.6	3.6	.2	-.63	.03	7.8	8.9	.06	24
6	PV-ChR2	5.6	1.1	2.5	.5	-.38	.11	8.2	7.4	-.05	25
7	PV-Arch	3.7	.4	19	2	.66	.04	7.8	8.6	.05	25
8	PV-Arch	14.1	.9	16.9	9	.08	.04	12.5	14.4	.07	23
9	Pyr-ChR2	5.6	1.1	4.9	.4	-.06	.1	8.3	7.0	-.08	19
10	Pyr-ChR2	6.8	.9	3.2	.5	-.35	.09	8.3	5.3	-.21	16
11	Pyr-ChR2	.7	1.9	11	2	.18	.15	9.4	12.8	.15	23
12	Pyr-ChR2	2.0	.01	3.4	.3	.26	.04	5.0	6.3	.11	26
13	Pyr-ChR2	3.1	.6	5.6	.9	.28	.11	6.7	7.5	.05	43
14	PV-ChR2	3.2	.3	3.2	.4	-.01	.07	6.7	6.9	.02	34
15	PV-ChR2	5.5	1.6	3.9	1.5	-.16	.23	10.3	5.5	-.3	16
16	PV-ChR2	9.6	1.9	10.2	.7	.03	.10	.9	5.6	-.11	14
17	PV-ChR2	2.0	.4	2.6	1.5	.13	.30	5.7	6.9	.10	15
18	PV-ChR2	7.6	1.4	9.5	.4	.10	.09	6.9	6.2	-.05	22
19	PV-ChR2	8.3	.5	8.4	.8	.01	.05	8.8	9.0	.01	39

S1 Table: Table containing mouse identity, type, relevant behavioral and neurometric thresholds, as well as number of recorded neurons. Neurometric threshold computed using Fisher information is scaled to an effective population size of 1000 neurons to control for differences in numbers of measured neurons.

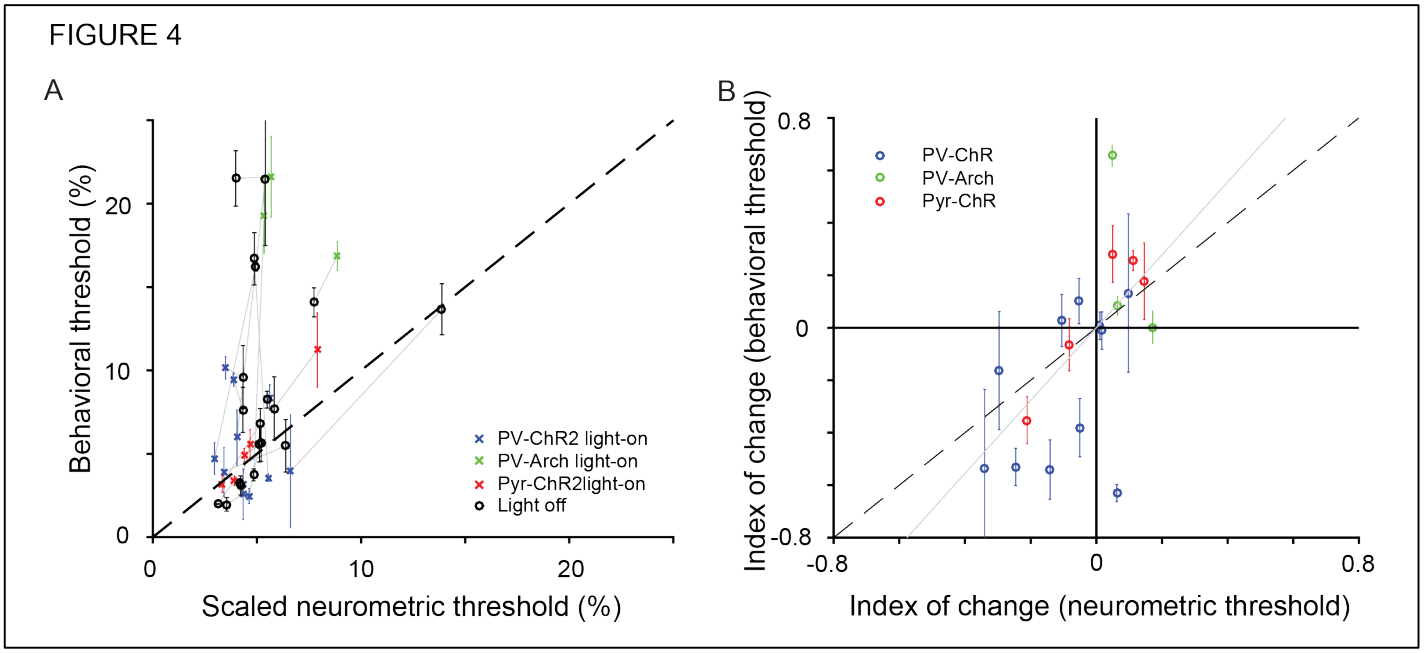

Figure 4. Changes in A1 tone responses due to optogenetic manipulations predict changes in behavioral frequency discrimination acuity across individuals.

A. Behavioral versus scaled neurometric frequency discrimination thresholds. Neurometric threshold (computed as inverse of Fisher information squared for tone-evoked responses from all neurons recorded in each mouse) is scaled to an effective population size of 1000 neurons to control for differences in numbers of measured neurons. Changing this scale factor is equivalent to changing y-axis labels. The scaled neurometric threshold based on the small recorded population was significantly (but weakly so, C=.37, p=0.02) correlated with the behavioral threshold (computed as the shift in frequency between the background and pre-pulse tone that evoked 50% of the maximum PPI). Each of 19 mice contributes 2 data points, representing the threshold computed on the basis of light-on and light-off trials. Gray lines connect light-on and light-off estimates for each mouse.

B. The index of change in neurometric threshold (difference between thresholds computed from data on light-on vs. light-off trials divided by the sum) was strongly correlated with the behavioral frequency discrimination (Correlation coefficient = 0.59, p=0.007). There is one data point for each mouse. Gray line is the best fit line through the origin. Behavioral errors were computed as described in the Methods.

Controls: effects of optogenetic manipulation on neural variability and correlations

Our model makes two assumptions that could be violated in neural systems: that cortical neurons obey Poisson statistics and that neural responses are independent of one another. In order to test the first assumption in our data, we measured the Fano factor of the recorded neurons. A large Fano factor indicates high neuronal variability [24]. The average Fano factor was around 1.2, similar to the value expected for Poisson neurons and to that previously measured across different cortical areas [25]. We found that none of the three optogenetic manipulations (PV-ChR2: $t_{335} = .4$, $p = .69$; PV-Arch: $t_{89} = .92$, $p = .36$; Pyr-ChR2: $t_{133} = -.2$, $p = .84$; Figure 5A-C) had a systematic effect on the distribution of Fano factors. This justified the original

analysis, in which neurons were treated as Poisson, both with and without optogenetic manipulation.

We next considered that neural variability has been observed to increase with the activity level of neurons [26]. It is plausible that the most active neurons, which have the largest impact on Fisher information, may be more variable than expected from the average Fano factor value. The Fisher information decreases as the Fano factor increases (Figure 5G), so higher variability in the most active neurons would disproportionately decrease the neurometric discriminability. To test whether this might be the case, we computed the neurometric thresholds using a generalized Poisson noise model that took into account the Fano factor of each recorded neuron separately. Neurometric thresholds using this model changed only slightly from the thresholds computed using the simple Poisson noise model (Figure 5H), again justifying our analysis.

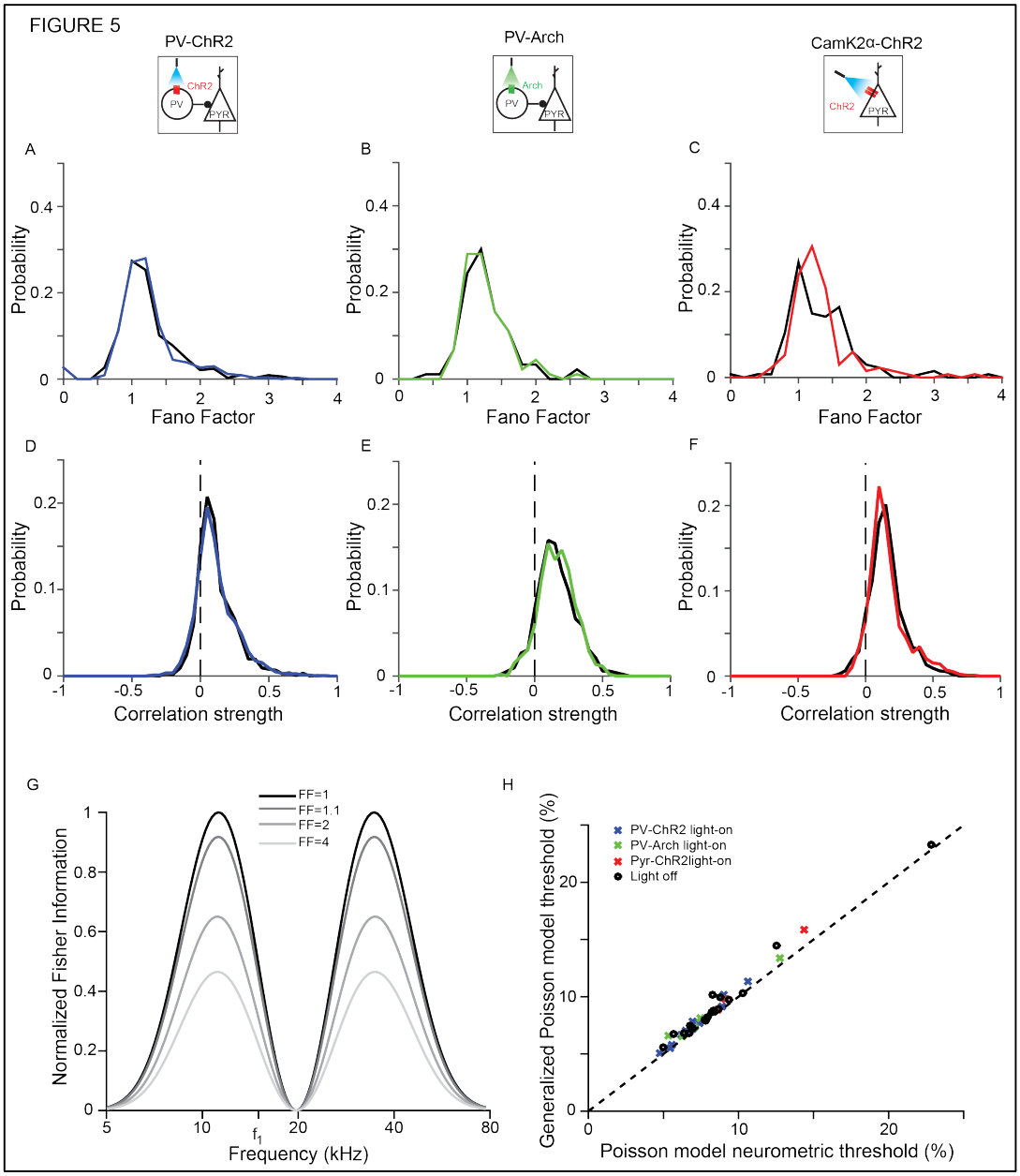

Figure 5. Optogenetic manipulations do not change neuronal variability or correlations.

A-C. Fano factor pooled across mice distributions are similar under light-on and light-off conditions. A: PV-ChR2, B: PV-Arch, C: CamK2a-ChR2. Black: light-off trials; Blue, Green, Red: light-on trials. Dots

D-F. Pairwise correlation distributions pooled across mice are similar under light-on and light-off conditions. D: PV-ChR2, E: PV-Arch, F: CamK2a-ChR2. Colors same as in A.

G. Increasing Fano factor reduces Fisher Information, shown here for a single neuron with Gaussian tuning curve (amplitude = 8 spikes/s, center frequency 20kHZ, tuning width = 0.2 decades) with a constant baseline (2 spikes/s).

H. Incorporating the measured Fano factors into our model of neuronal firing via a generalized Poisson model has a weak effect on the predicted threshold.

We also measured the strength of pairwise neural correlations, and observed they tended to be small but positive ($\bar{C}_{PV-ChR2} = .09,\ t_{1937} = 28,\ p = 4.6 * 10^{-141}$; $\bar{C}_{PV-Arch} = .13,\ t_{524} = 22,\ p = 2.2 * 10^{-76}$; $\bar{C}_{Pyr-ChR2} = .13,\ t_{982} = 32,\ p = 1.1 * 10^{-155}$). The optogenetic manipulations had no systematic effect on the distribution of correlations (paired *t* test ns: PV-ChR2 $t_{1937} = .26,\ p = .80$; PV-Arch $t_{524} = -1.3,\ p = .18$; Pyr-ChR2 $t_{982} = -1.7,\ p = .09$; see Figure 5D-F, S1). Correlations in similar models have been observed to lead only to small increases in population-level discrimination threshold [27]. The small changes in threshold observed in previous work, in addition to the negligible change in the correlation distribution that we observe upon optogenetic manipulation, make it unlikely that correlations account for the neurometric threshold changes that we see when cortex is manipulated.

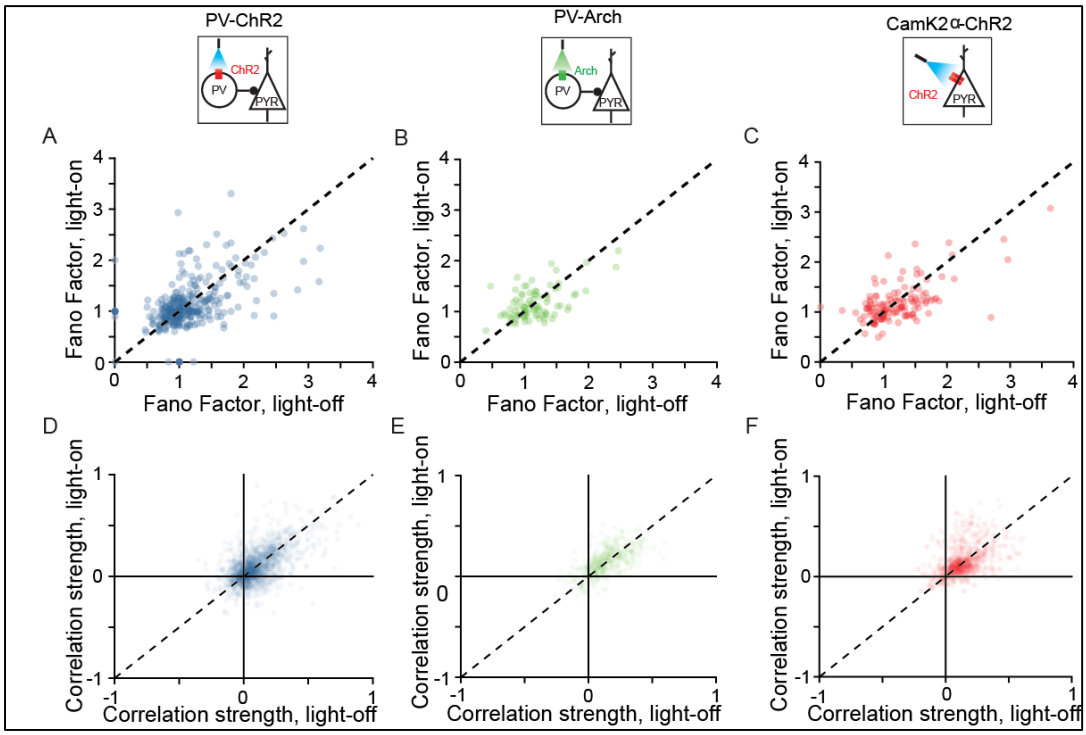

S1 Figure: Fano factor and correlation scatter plots comparing light-on and light-off conditions. **A-C**: Fano factor with and without light on for PV-ChR2, PV-Arch, and Pyr-ChR2 mice, respectively. **D**-F: Pairwise correlations with and without light on for PV-ChR2, PV-Arch, and Pyr-ChR2 mice, respectively.

Discussion.

Theory has shown that providing inputs to inhibitory neurons in a balanced excitatory-inhibitory network can lead to either a decrease, or, paradoxically, an increase of excitatory responses, depending on the specifics of recurrent coupling in the network and the strength of the manipulation of inhibitory activity [16]. By examining changes evoked by optogenetic

manipulations across subjects, we find that modifications of the excitatory-inhibitory interactions in auditory cortex drive diverse, and sometimes opposite, changes in tone-evoked responses across individuals. Remarkably, we found a strong correlation between these changes in neuronal populations, and behavioral changes in the acuity of frequency discrimination by individual mice. Thus our results demonstrate that the same optogenetic manipulations of excitatory and inhibitory neuronal activity in different individuals, can have diverse effects on sensory discrimination. More generally, these findings support a role for excitatory-inhibitory networks in the cortex in mediating sensory discrimination.

Where does this variability in the effects of manipulations across animals arise from? Some of the differences may be due to the inherent variability in circuitry across animals: the excitatory-inhibitory circuit can have different connectivity patterns, and animals may exhibit differences in frequency sensitivity due to a combination of genetic and environmental factors. In addition, optogenetic manipulations introduce variability across animals due to technical limitations of the technique. In testing the function of specific neuronal cell types in sensory processing, there are a number of potential confounds. For example, the exact position of the needle for virus injection within AC, the depth of penetration, and the spread of the virus, can all skew the extent to which the virus is expressed within AC. The position of the optic cannula relative to the spread of the virus injection as well as the recording electrode would affect how many neurons are stimulated and how strongly, and also how many of those neurons are being picked up by the recording. Small changes in any of these parameters can potentially lead to strong differences in the functional effects of optogenetic perturbations, activating a different fraction of neurons across different laminae, and in different tonotopic regions of the cortex. In this study, we capitalized on these differences because they allowed us to assay the range of potential effects of optogenetic manipulations. It was critical, however, to ensure that within animals, optogenetic manipulation would produce the same effect during behavioral testing and during electrophysiological recordings. We therefore used an implanted optic cannula and a light delivery system with the same settings to deliver light both during the electrophysiological recording and the behavioral measurements, so that stimulation parameters were the same for both.

Our results provide insight into potential role of cortical inhibition in shaping frequency discrimination behavior. Cortical inhibitory neurons have been hypothesized to modulate numerous aspects of tone-evoked responses in the excitatory cortical circuit, such as tuning width, reliability of firing, tone-evoked response strength, and correlations in firing rate activity [2, 19, 28]. Neurons in the auditory cortex change their tuning properties with learning, attention or experience [29-35], suggesting that these changes can underlie changes in auditory perception.

368 Indeed, AC was shown to play an important function in enabling learning-driven changes in
369 auditory processing [17, 36]. Our present work demonstrates that modulation of excitatory-
370 inhibitory dynamics can in principle support a wide range of modulatory effects on auditory
371 frequency discrimination behavior.

372 The limited size of our recordings of 10-100 frequency-tuned neurons per animal precluded
373 direct prediction of behavioral thresholds: an extrapolation from the measured population
374 indicates that O(1000) neurons would be required to fully account for behaviorally observed
375 frequency discrimination threshold (S2 Figure). This observation is consistent with an anatomical
376 estimate suggesting that O(1000) neurons in the mouse AC are responsive to a given tone
377 (mouse cortex has ~10^5 neurons/mm^3 [37], the AC is ~5 mm^3 in size, ~30-50% of neurons are
378 frequency tuned, and the tuning width is ~1/10 of the auditory spectrum). The fact that we were
379 able to make strong predictions about optogenetic effects on behavior despite this sub-sampling
380 suggests that the changes we observed in the measured cortical neurons were representative of
381 changes occurring across the entire AC. Comprehensive recordings or imaging of more complete
382 populations of AC neurons will enable a test of the hypothesis that frequency discrimination
383 performance is limited by the encoding at the cortical level.

384 We observed a relationship between neural responses and behavior under the specific
385 conditions of optogenetic manipulations of cortex, but the methods used here will be broadly
386 useful for understanding other complex phenomena. For example, consider appetitive and
387 aversive conditioning which have been shown to effect cortical remapping [31, 38, 39], while
388 leading to diverse behavioral responses [9, 17]. In particular, such remapping leads to an
389 overrepresentation of the aversive stimulus in cortex, but while some animals show improved
390 frequency discrimination acuity, others are impaired. In fact, our results indeed show that different
391 ways over-representing the aversive stimulus can lead to improved or impaired acuity, depending
392 on the details of the change (Figure 6). For example, shifting the neural tuning curves towards the
393 aversive frequency leads to increased sensitivity near this tone (Figure 6B), while simply
394 increasing neural activity in response to tones near the aversive frequency can lead to impaired
395 discrimination (Figure 6C). Fisher information analyses which we used in our paper have proven
396 generally useful in understanding neural coding, providing insight about sound localization
397 strategies [40], sensitivity to variations in sound levels [41], habituation to repeated sounds [42],
398 detection of sound in noise [43] and heading perception [27]. Our method allows applications of
399 this technique to compare behavioral discrimination thresholds to neurometric uncertainty in tone
400 frequency estimation.

Whereas we used responses to single tones as the stimulus in this study, AC neurons generally respond to more complex sounds in a manner that is not well explained by the single-tone responses [44, 45]. Our methods could be used to probe the fidelity of cortical representation and behavior in response to any parameterized space of auditory stimuli, e.g. auditory textures, phonemes, or overtone profiles. Similarly to work in visual texture perception [46, 47], one could test the discrimination thresholds along different dimensions of the texture space [48-50]. Changes in these thresholds due to optogenetic circuit manipulation could then be compared with changes in a neurometric threshold based on Fisher Information, as applied here. Such studies will elucidate the role of AC in facilitating complex auditory discrimination.

Viewed in aggregate in terms of a mean over individuals, our results would have yielded small average effects with large individual variations appearing as “noise’’. Averaging in this way would have obscured the function of AC in frequency discrimination because the correlation between individual circuit changes and individual behavioral changes would have been missed. It is only by treating the mice as individuals that we were able to understand the general role auditory cortex plays in shaping the response. We suggest that such attention to individual variation will be broadly important throughout neuroscience as large-scale recordings begin to reveal the neural basis of behavioral diversity.

FIGURE 6

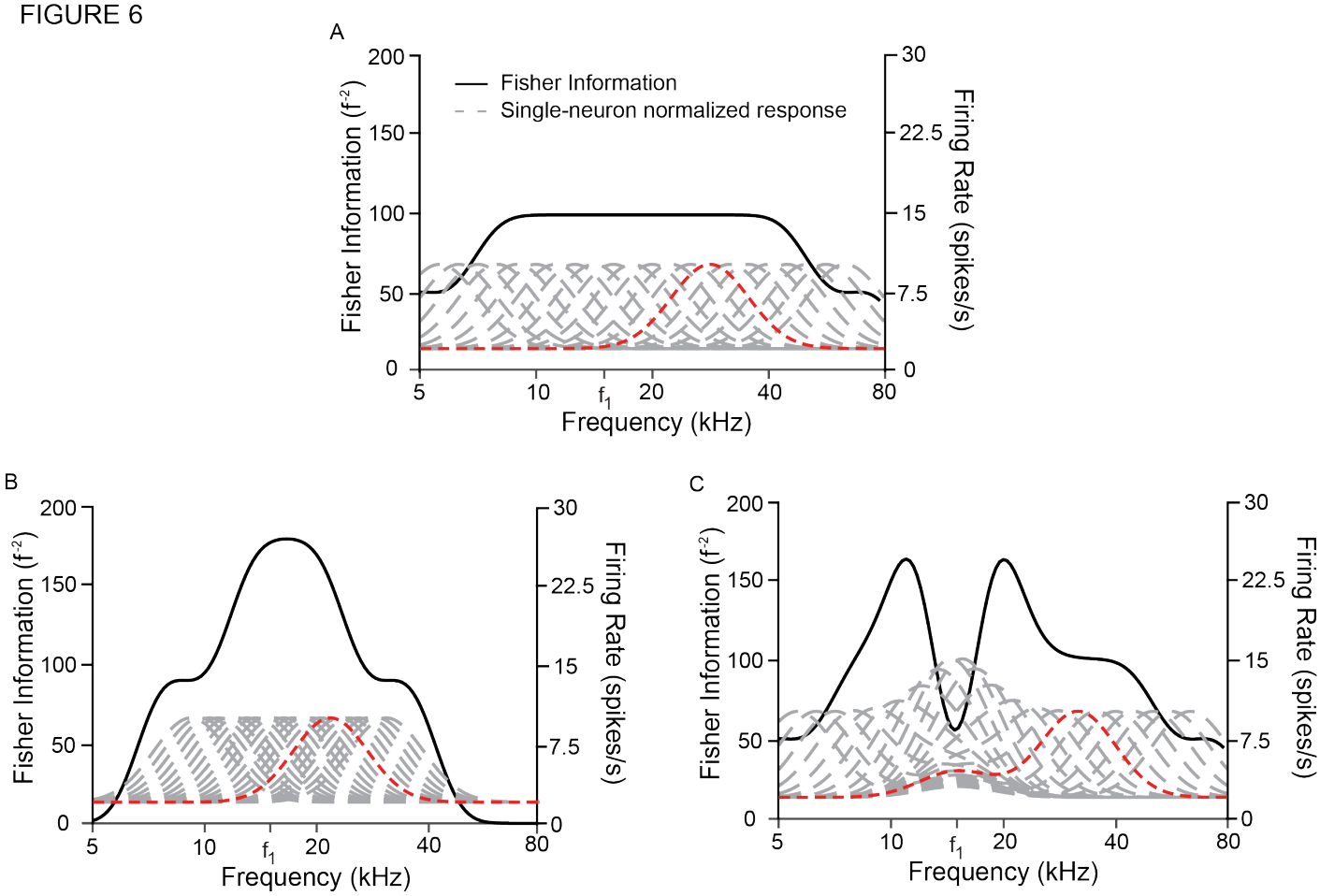

Figure 6. Overrepresenting a specific frequency can increase or reduce sensitivity to that frequency.

A. Fisher information (black) computed from a homogeneous population of neurons (responses in gray) has an even sensitivity across a broad range of frequencies. A sample tuning curve (red) is used to illustrate neural transformations in **B** and **C**. Neurons have baseline activity of 2 spikes/s, peak response of 10 spikes/s, peak frequency spaced 1/20th of a decade apart, with HWHM of .1 decades.

B. Fisher information is plotted for a neural population overrepresenting frequency f_1 by shifting peak frequencies halfway between their original location in **A** and f_1. Fisher information approximately doubles near f_1, but is reduced near the edges.

C. Fisher information is plotted for a neural population overrepresenting frequency f_1 by adding a Gaussian bump near f_1 with an amplitude that diminishes with distance between the preferred frequency of the neuron and f_1. Fisher information is *diminished* at f_1, leading to reduced sensitivity at this frequency, despite its overrepresentation within the population firing activity.

436 ## Methods.

437 *Animals.* All experiments were performed in adult male mice (supplier - Jackson Laboratories; age, 12-15
438 weeks; weight, 22-32 g; PV-Cre mice, strain: B6; 129P2-Pvalbtm1(cre)Arbr/J; CamKIIα-Cre: B6.Cg-
439 Tg(CamKIIα-Cre)T29-1Stl/J) housed at 28° C on a 12h light:dark cycle with water and food provided *ad*
440 *libitum*, 5 or fewer animals per cage. All animal work was conducted according to the guidelines of
441 University of Pennsylvania IACUC and the AALAC Guide on Animal Research. Anesthesia by isofluorane
442 and euthanasia by carbon dioxide were used. All means were taken to minimize the pain or discomfort of
443 the animals during and following the experiments. Experiments were performed as described previously
444 [9].

445 *Viral constructs.* Modified AAV vectors were obtained from Penn VectorCore. To suppress PVs, we used
446 modified AAV vector encoding Archaerhodopsin (Arch) under FLEX design (Addgene plasmid 22222,
447 AAV-FLEX-Arch-GFP [51]. To activate either PVs iin PV-Cre mice and or excitatory neurons in CamKIIα-
448 Cre mice, we used modified AAV encoding ChR2 under FLEX design (Addgene plasmid 18917 AAV-
449 FLEX-ChR2- tdTomato, ChR2 [52]. As a control, we used modified AAV vectors encoding only GFP or
450 tdTomato under FLEX design.

451 *Experimental methods overview.* Methods have been previously described [9]. Briefly, at least 10 days
452 prior to the start of experiments, mice were injected with a viral construct, if any, and implanted with optical
453 cannulas, and a headpost, as previously described, under isoflurane anesthesia. Viral construct injection
454 targeted AC using stereotaxic map. Fiber-optic cannulas were implanted bilaterally over the injection site
455 at depth of 0.5 mm from the scull surface, along the dorsal-ventral axis. After recovery, mice were
456 habituated to the head-fixing apparatus, and subjected to behavioral frequency discrimination tests for 1-3
457 days, followed by electrophysiological recordings in the auditory cortex. On half of the trials in behavioral
458 and neurophysiological recordings, light was presented through the fiber-optic cannula to activate or
459 suppress target neurons. Upon conclusion of experiments, brains were extracted, fixed and subjected to
460 immunostaining. Viral spread was confirmed postmortem by visualization of the fluorescent protein
461 expression in fixed brain tissue, and its co-localization with PV or excitatory neurons, following immuno-
462 histochemical processing with the appropriate antibody.

463 *Behavioral frequency discrimination.* Behavioral frequency discrimination was measured using a modified
464 PPI procedure on daily basis [9, 53]. As previously reported [9, 17], PPI provides psychometric response
465 curves for frequency discrimination over the course of a single session that lasts less than 1 h and does
466 not require training the subject, which can confound interpretation of fear conditioning. Mice were head-
467 fixed, connected to optical cannulas as needed, and placed on a load-bearing platform. Sound was
468 presented through a speaker, consisting of a background tone (15kHz, 10-20 s, 80 dB SPL) that, on each
469 trial, switched to a pre-pulse tone (10.2, 12.6, 13.8, 14.7, and 15.0 kHz, 60 ms, 80 dB SPL) followed by
470 startle noise (SS, broad-band noise, 100 dB SPL, 20 ms). The frequency difference between the
471 background and pre-pulse tone is denoted Δf. Each session started with presentation of 10 startle-only

472 trials, to ensure that the mouse habituated to the beginning of the session. Data from these trials were not
473 used for the analysis. Each pre-pulse tone was repeated in a pseudo-random order at least 5 times during
474 each behavioral session.
475 The Acoustic Startle Response (ASR) for a given Δf was computed as the average over trials of the
476 difference between the maximum vertical force applied within the 500 ms window following SS and the
477 average baseline activity during 500 ms prior to SS. In each PPI session, the PPI was calculated as:

478 $$PPI(\Delta f) = 100\frac{ASR(0) - ASR(\Delta f)}{ASR(0)}$$

479 where PPI is reported in % relative to maximum *PPI*, and $ASR(\Delta f)$ is measured using the 50% of the
480 strongest ASR magnitudes for each PP frequency. 50% is chosen for consistency with previous work, as
481 the psychometric curve has the steepest slope at this value [17]. Behavioral threshold was determined by
482 fitting the PPI with a generalized logistic function, and defining the threshold for the fit as the Δf that
483 produced 50% of the maximum PPI. Because the primary source of uncertainty related to how close the
484 animal's threshold was to sampled points, we computed thresholds for the set of fits producing less than a
485 25% increase in MSE relative to the best fit (although increasing this cutoff to 60% yielded small
486 differences). We took the mean and standard deviation of the resulting set of thresholds to reflect the
487 animal's threshold. Each psychometric functions consisted of 5 data points representing the difference
488 between the background frequency and 5 prepulse frequencies (PP). Each data point was obtained by
489 averaging ASRs from all repetitions corresponding to a given frequency. In a standard PPI session, 20
490 repetitions of each PP were presented (100 trials in total). However, if either threshold was out of the
491 range (0.5–32%) or the fit coefficient of the curve (R^2) was below 0.7, the mouse underwent an additional
492 10 repetitions (50 trials). If threshold and fit curve failed to meet the above criteria after 200 trials, the
493 session was excluded from statistical analysis (3 out of 61 sessions). Previous studies have shown that
494 psychometric thresholds obtained from day-to-day measurements were stable [9, 17, 54]. Light-on trials
495 included a 1s laser presentation that starts 0.5 s preceding PP onset. Light-off trials included laser
496 presentation at quasi-random position during ITI. All analysis was performed separately on light-on and
497 light-off trials. Simple randomization was used to assign the subjects to the experimental groups. A
498 pseudorandom sequence was used for tone presentation during PPI tests. During PPI procedure, the
499 timing of the laser presentation on Laser-off trials was pseudo-randomized with respect to the timing of the
500 tones. Blinding of experiment with respect to animal groups was not possible as animals in different
501 groups underwent different experimental protocols.
502 *Neuronal tone response measurement.* All recordings were carried out inside a double-walled acoustic
503 isolation booth (Industrial Acoustics) as previously described [9]. Activity of neurons in the primary auditory
504 cortex of head-fixed, awake mice was recorded via a silicon multi-channel probe (Neuronexus). Putative
505 principal (excitatory) neurons were identified using waveform and spontaneous firing rate (for details see
506 [9]). Acoustic stimulus was delivered via a calibrated magnetic speaker (Tucker-Davis Technologies) [45].
507 We measured the frequency tuning curves by presented a train of 50 pure tones (50ms long, ISI 450 ms)

with frequencies spaced logarithmically between 1 and 80 kHz and at 8 intensities (sound pressure levels, SPLs) spaced uniformly between 10 and 80 dB, a standard procedure in characterizing auditory responses, and determined the threshold amplitude for tone at each frequency for each neuron [9, 45]. For data analysis we averaged responses of the neurons to each tone across 3 highest amplitudes. Each tone was repeated twice in pseudo-random sequence and the stimulus was counter-balanced for laser presentation. On light-on trials, light was presented via the optic cannulas, with the onset of 100 ms prior to tone onset, and lasting for 250 ms. The full stimulus was repeated 5 times.

Histology. Virus spread was confirmed postmortem by visualization of the fluorescent protein expression in fixed brain tissue, and its colocalization with PV or excitatory neurons, following immuno-histochemical processing with the appropriate antibody.

Identification of Putative Excitatory Neurons. Putative principal (excitatory) neurons were identified using waveform and spontaneous firing rate (for details see Aizenberg et al., 2015).

Neural Response Analysis. The neural frequency response function was calculated using the average frequency tuning curve across the three highest intensities. The results were modeled using a Gaussian in log-frequency space:

$$FR(f) = B + A * \exp\left[-\frac{(f - f_0)^2}{2\sigma^2}\right]$$

where B represents the baseline response, A represents the amplitude of the strongest evoked response (relative to baseline), f_0 represents the frequency evoking the strongest response, and σ corresponds to the width of the frequency response function. Only neurons whose Gaussian fit had $R^2 > .6$ were kept for further analysis.

In order to calculate Fano factor of a neuron, we calculated mean and variance of the firing rate to each combination of frequency and SPL. The slope of these data was taken as an estimate of Fano factor.

The correlation between neurons (calculated only between simultaneously recorded neurons) was computed using a reduced measure of deviation from the mean for each neuron:

$$s_i^k(f,d) = \frac{r_i^k(f,d) - \overline{r_i}(f,d)}{\sqrt{F_i \overline{r_i}(f,d)}}$$

where k denotes the repetition number (1-5), i denotes the neuron, f denotes the frequency, d denotes the intensity, r denotes the evoked response, $\bar{r}$ denotes the average response (firing rate) of a neuron to a particular frequency and intensity, and F denotes the Fano factor of that neuron. For a generalized Poisson process, s_i has zero mean and unit variance because the variance is proportional to the mean. The correlation between two neurons is then given by

$$C_{i,j} = \langle s_i^k(f,d) s_j^k(f,d) \rangle_{k,f,d}$$

Computing Fisher Information. Fisher information was calculated to provide a measure of neurometric frequency discrimination. Fisher information was calculated numerically from the recorded data based on the characterization of the neural responses (see *Neural Response Analysis*), and is given by:

$$I_F(f) = \sum_{\vec{n}} P(\vec{n}|f) \left(\frac{\partial}{\partial f} \log P(\vec{n}|f)\right)^2$$

where *P* is the probability that the population of neurons produces $\vec{n}$ = *(n₁, n₂,…)* spikes in response to the tone f. Assuming Poisson variability and independent neurons,

$$P(\vec{n}|f) = \prod_i P(n_i|f) = \prod_i \frac{e^{-\mu_i(f)}\mu(f)^{n_i}}{n_i!}$$

where the first equation expresses the independent neuron assumption and the second step uses the assumption of Poisson variability. Here, μ_i and n_i are the expected and observed number of spikes from neuron i, respectively. For mice where multiple recording sessions were performed, neurons were pooled across sessions. A second model assumes independent neurons and uses a generalized Poisson distribution:

$$P(n_i|f) = \frac{\alpha_i(f)(\alpha_i(f) + n_i\lambda_i)^{n-1}e^{-(\alpha_i(f)+n_i\lambda_i)}}{n_i!}$$

where $\alpha_i = \mu_i(f) * F_i^{-1/2}$ and $\lambda_i = 1 - F_i^{-1/2}$. This model only allows for Fano factors above 1, which is consistent with other models of neural variability and measured cortical variability [24, 26]. We therefore set any measured Fano factor less than 1 to exactly 1 for the purpose of the Fisher information calculation.

<u>*Estimating the number of neurons for neurometric thresholds.*</u> Animals displayed varying levels of frequency discrimination acuity, and we measured different sized subsets of frequency-tuned neurons in each experiment. In order to estimate the number of neurons required to account for behavioral discrimination acuity from the measured population, we utilized the fact that Fisher information for a population of independent neurons is the sum of the Fisher information from each neuron.

$$I^{(total)} = \sum_n I^{(n)}$$

We then assume that the population of neurons that we measured are representative of the overall population (at least the population that contributes to discrimination at the relevant frequency).

$$I^{(n)} \approx \frac{1}{N_E}\sum_{k=1}^{N_E} I_E^{(k)} = \frac{1}{N_E} I_E^{(total)}$$

Here we use n to refer to the overall population that we seek to estimate, k to index the neurons that were measured, N_E is the number of frequency-tuned neurons measured in a specific mouse, $I_E^{(k)}$ is the Fisher information of these experimentally measured neurons, and $I_E^{(total)}$ is the total information used to calculate the neurometric threshold. Recalling that the neurometric threshold is defined as $I^{-1/2}$, we then have

$$I^{(total)} = \frac{N_T}{N_E} I_E^{(total)}$$

We can rewrite this as

$$N_T = N_E \left(\frac{t_{beh}}{t_{neu}}\right)^2$$

572 where t_{beh} is this behaviorally measured threshold and t_{neu} is the neurometric estimate of the threshold.
573 This is plotted for each animal used in our analyses in S2 Figure, and we find that the average for both
574 light-on and light-off conditions is just about 10^3 neurons.

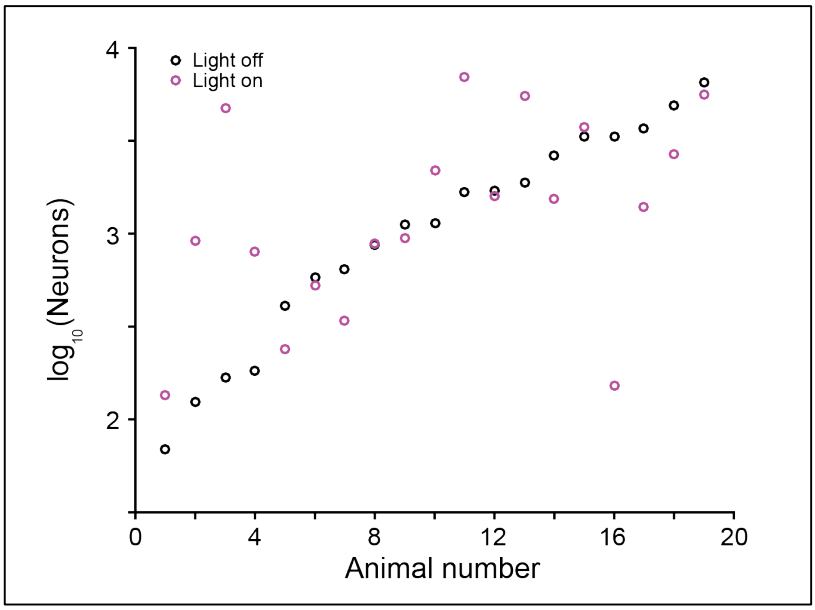

575

576 *S2 Figure.* Number of frequency-tuned neurons required to account for behavioral sensitivity for each
577 mouse. Average of both light-on and light-off conditions is ~10^3 neurons.
578
579 *Comparing behavioral and neurometric thresholds.* Neural responses were accumulated over all recording
580 sessions for each mouse, and used to compute the Fisher information for the animal. The Fisher
581 information provides a bound on the variability of an unbiased estimator, and any criterion level of
582 decoding performance scales with the inverse-square root of the Fisher information. If neural responses
583 are independent, the Fisher information scales linearly with the number of neurons. In order to compare
584 threshold predictions between mice with different numbers of measured neurons, we computed the
585 average Fisher information per neuron. This allowed us to compare across mice and to estimate the
586 minimum number of effective frequency-tuned neural units that must contribute to explain the observed
587 frequency discrimination performance [18]. To estimate the neurometric threshold, we first computed the
588 inverse square root of the Fisher information per neuron, and took an average over a small region around
589 15 kHz (the baseline frequency used in behavioral tests). Only mice with more than 10 recorded
590 frequency-tuned neurons were included in the analysis (19 mice). Our estimate is a lower limit on the
591 uncertainty in the estimate of this tone frequency based on the recorded population responses. Since
592 Fisher information scales linearly in an independent population, this method also provides an estimate on
593 the effective number of neurons which must contribute to the tone representation in order to account for
594 behavioral discriminability (S2 Figure). The observed neurometric discriminability with order one thousand
595 independent neurons is similar to behavioral discrimination acuity.
596 *Data availability.* All relevant data will be deposited in the Dryad database and made publically available.
597 *Code availability.* All relevant code will be posted on Github and made publically available.

Supplementary Information.

S1 Table: Table containing mouse identity, type, relevant behavioral and neurometric thresholds, as well as number of recorded neurons. Neurometric threshold computed using Fisher information is scaled to an effective population size of 1000 neurons to control for differences in numbers of measured neurons.

S1 Figure: Fano factor and correlation scatter plots comparing light-on and light-off conditions. **A**-**C**: Fano factor with and without light on for PV-ChR2, PV-Arch, and Pyr-ChR2 mice, respectively. **D**-F: Pairwise correlations with and without light on for PV-ChR2, PV-Arch, and Pyr-ChR2 mice, respectively.

S2 Figure. Number of frequency-tuned neurons required to account for behavioral sensitivity for each mouse. Average of both light-on and light-off conditions is ~10^3 neurons.

615 ## References

616

617 1. Isaacson JS, Scanziani M. How inhibition shapes cortical activity. Neuron. 2011;72(2):231-43. Epub
618 2011/10/25. doi: 10.1016/j.neuron.2011.09.027. PubMed PMID: 22017986; PubMed Central PMCID:
619 PMC3236361.
620 2. Froemke RC. Plasticity of cortical excitatory-inhibitory balance. Annu Rev Neurosci. 2015;38:195-
621 219. Epub 2015/04/22. doi: 10.1146/annurev-neuro-071714-034002. PubMed PMID: 25897875.
622 3. Lee SH, Kwan AC, Zhang S, Phoumthipphavong V, Flannery JG, Masmanidis SC, et al. Activation of
623 specific interneurons improves V1 feature selectivity and visual perception. Nature. 2012;488(7411):379-
624 83. Epub 2012/08/11. doi: 10.1038/nature11312. PubMed PMID: 22878719; PubMed Central PMCID:
625 PMC3422431.
626 4. Wilson NR, Runyan CA, Wang FL, Sur M. Division and subtraction by distinct cortical inhibitory
627 networks in vivo. Nature. 2012;488(7411):343-8. Epub 2012/08/11. doi: 10.1038/nature11347. PubMed
628 PMID: 22878717; PubMed Central PMCID: PMC3653570.
629 5. Marlin BJ, Mitre M, D'Amour J A, Chao MV, Froemke RC. Oxytocin enables maternal behaviour by
630 balancing cortical inhibition. Nature. 2015;520(7548):499-504. Epub 2015/04/16. doi:
631 10.1038/nature14402. PubMed PMID: 25874674; PubMed Central PMCID: PMC4409554.
632 6. Atallah BV, Bruns W, Carandini M, Scanziani M. Parvalbumin-expressing interneurons linearly
633 transform cortical responses to visual stimuli. Neuron. 2012;73(1):159-70. doi:
634 10.1016/j.neuron.2011.12.013. PubMed PMID: 22243754; PubMed Central PMCID: PMC3743079.
635 7. Seybold BA, Phillips EA, Schreiner CE, Hasenstaub AR. Inhibitory Actions Unified by Network
636 Integration. Neuron. 2015;87(6):1181-92. Epub 2015/09/25. doi: 10.1016/j.neuron.2015.09.013. PubMed
637 PMID: 26402602.
638 8. Phillips EA, Hasenstaub AR. Asymmetric effects of activating and inactivating cortical interneurons.
639 Elife. 2016;5. doi: 10.7554/eLife.18383. PubMed PMID: 27719761.
640 9. Aizenberg M, Mwilambwe-Tshilobo L, Briguglio JJ, Natan RG, Geffen MN. Bidirectional Regulation
641 of Innate and Learned Behaviors That Rely on Frequency Discrimination by Cortical Inhibitory Neurons.
642 PLoS Biol. 2015;13(12):e1002308. Epub 2015/12/03. doi: 10.1371/journal.pbio.1002308. PubMed PMID:
643 26629746; PubMed Central PMCID: PMC4668086.
644 10. Natan RG, Briguglio JJ, Mwilambwe-Tshilobo L, Jones SI, Aizenberg M, Goldberg EM, et al.
645 Complementary control of sensory adaptation by two types of cortical interneurons. eLife. 2015;4:pii:
646 e09868. Epub 2015/10/16. doi: 10.7554/eLife.09868. PubMed PMID: 26460542; PubMed Central PMCID:
647 PMC4641469.
648 11. Boyden ES, Zhang F, Bamberg E, Nagel G, Deisseroth K. Millisecond-timescale, genetically targeted
649 optical control of neural activity. Nat Neurosci. 2005;8(9):1263-8. doi: 10.1038/nn1525. PubMed PMID:
650 16116447.
651 12. Zhang F, Wang LP, Brauner M, Liewald JF, Kay K, Watzke N, et al. Multimodal fast optical
652 interrogation of neural circuitry. Nature. 2007;446(7136):633-9. doi: 10.1038/nature05744. PubMed
653 PMID: 17410168.
654 13. Sohal VS, Zhang F, Yizhar O, Deisseroth K. Parvalbumin neurons and gamma rhythms enhance
655 cortical circuit performance. Nature. 2009;459(7247):698-702. Epub 2009/04/28. doi:
656 10.1038/nature07991. PubMed PMID: 19396159.
657 14. Cardin J, Carlen M, Meletis K, Knoblich U, Zhang F, Deisseroth K, et al. Targeted optogenetic
658 stimulation and recording of neurons in vivo using cell-type-specific expression of Channelrhodopsin-2.
659 Nature protocols. 2010;5(2):247-54. doi: 10.1038/nprot.2009.228.

660 15. Deisseroth K. Optogenetics. Nat Methods. 2011;8(1):26-9. Epub 2010/12/31. doi:
661 10.1038/nmeth.f.324. PubMed PMID: 21191368.
662 16. Tsodyks MV, Skaggs WE, Sejnowski TJ, McNaughton BL. Paradoxical effects of external modulation
663 of inhibitory interneurons. J Neurosci. 1997;17(11):4382-8. PubMed PMID: 9151754.
664 17. Aizenberg M, Geffen MN. Bidirectional effects of auditory aversive learning on sensory acuity are
665 mediated by the auditory cortex. Nature neuroscience. 2013;16:994-6.
666 18. Cover TM, Thomas JA. Elements of Informatioin Theory. New York: Wiley; 1991.
667 19. Wang J, Caspary D, Salvi RJ. GABA-A antagonist causes dramatic expansion of tuning in primary
668 auditory cortex. Neuroreport. 2000;11(5):1137-40. PubMed PMID: 10790896.
669 20. Wang J, McFadden SL, Caspary D, Salvi R. Gamma-aminobutyric acid circuits shape response
670 properties of auditory cortex neurons. Brain Res. 2002;944(1-2):219-31. PubMed PMID: 12106684.
671 21. Chen QC, Jen PH. Bicuculline application affects discharge patterns, rate-intensity functions, and
672 frequency tuning characteristics of bat auditory cortical neurons. Hear Res. 2000;150(1-2):161-74.
673 PubMed PMID: 11077201.
674 22. Wehr M, Zador AM. Balanced inhibition underlies tuning and sharpens spike timing in auditory
675 cortex. Nature. 2003;426(6965):442-6. Epub 2003/12/04. doi: 10.1038/nature02116. PubMed PMID:
676 14647382.
677 23. Danskin B, Denman D, Valley M, Ollerenshaw D, Williams D, Groblewski P, et al. Optogenetics in
678 Mice Performing a Visual Discrimination Task: Measurement and Suppression of Retinal Activation and
679 the Resulting Behavioral Artifact. PLoS One. 2015;10(12):e0144760. doi: 10.1371/journal.pone.0144760.
680 PubMed PMID: 26657323; PubMed Central PMCID: PMCPMC4686123.
681 24. Blackwell JM, Taillefumier TO, Natan RG, Carruthers IM, Magnasco MO, Geffen MN. Stable
682 encoding of sounds over a broad range of statistical parameters in the auditory cortex. Eur J Neurosci.
683 2016;43(6):751-64. doi: 10.1111/ejn.13144. PubMed PMID: 26663571.
684 25. Churchland MM, Yu BM, Cunningham JP, Sugrue LP, Cohen MR, Corrado GS, et al. Stimulus onset
685 quenches neural variability: a widespread cortical phenomenon. Nat Neurosci. 2010;13(3):369-78. doi:
686 10.1038/nn.2501. PubMed PMID: 20173745; PubMed Central PMCID: PMCPMC2828350.
687 26. Goris RL, Movshon JA, Simoncelli EP. Partitioning neuronal variability. Nat Neurosci.
688 2014;17(6):858-65. doi: 10.1038/nn.3711. PubMed PMID: 24777419; PubMed Central PMCID:
689 PMCPMC4135707.
690 27. Gu Y, Fetsch CR, Adeyemo B, Deangelis GC, Angelaki DE. Decoding of MSTd population activity
691 accounts for variations in the precision of heading perception. Neuron. 2010;66(4):596-609. doi:
692 10.1016/j.neuron.2010.04.026. PubMed PMID: 20510863; PubMed Central PMCID: PMCPMC2889617.
693 28. Wang J, McFadden SL, Caspary D, Salvi R. Gamma-aminobutyric acid circuits shape response
694 properties of auditory cortex neurons. Brain Res. 2002;944(1-2):219-31. Epub 2002/07/11. PubMed PMID:
695 12106684.
696 29. Froemke RC, Carcea I, Barker AJ, Yuan K, Seybold BA, Martins AR, et al. Long-term modification of
697 cortical synapses improves sensory perception. Nat Neurosci. 2013;16(1):79-88. Epub 2012/11/28. doi:
698 10.1038/nn.3274. PubMed PMID: 23178974.
699 30. Kilgard MP, Merzenich MM. Order-sensitive plasticity in adult primary auditory cortex. Proc Natl
700 Acad Sci U S A. 2002;99(5):3205-9. Epub 2002/03/07. doi: 10.1073/pnas.261705198. PubMed PMID:
701 11880653; PubMed Central PMCID: PMC122497.
702 31. Polley D, Steinberg E, Merzenich M. Perceptual learning directs auditory cortical map
703 reorganization through top-down influences. J Neurosci. 2006;26(18):4970-82. doi:
704 10.1523/jneurosci.3771-05.2006.
705 32. Recanzone GH, Merzenich MM, Schreiner CE. Changes in the distributed temporal response
706 properties of SI cortical neurons reflect improvements in performance on a temporally based tactile
707 discrimination task. J Neurophysiol. 1992;67(5):1071-91. Epub 1992/05/01. PubMed PMID: 1597698.

33. Fritz J, Shamma S, Elhilali M, Klein D. Rapid task-related plasticity of spectrotemporal receptive fields in primary auditory cortex. Nat Neurosci. 2003;6(11):1216-23. Epub 2003/10/30. doi: 10.1038/nn1141. PubMed PMID: 14583754.
34. Fritz JB, Elhilali M, Shamma SA. Differential dynamic plasticity of A1 receptive fields during multiple spectral tasks. J Neurosci. 2005;25(33):7623-35. Epub 2005/08/19. doi: 10.1523/JNEUROSCI.1318-05.2005. PubMed PMID: 16107649.
35. Znamenskiy P, Zador AM. Corticostriatal neurons in auditory cortex drive decisions during auditory discrimination. Nature. 2013;497(7450):482-5. Epub 2013/05/03. doi: 10.1038/nature12077. PubMed PMID: 23636333; PubMed Central PMCID: PMC3670751.
36. Bajo VM, Nodal FR, Moore DR, King AJ. The descending corticocollicular pathway mediates learning-induced auditory plasticity. Nat Neurosci. 2010;13(2):253-60. Epub 2009/12/29. doi: 10.1038/nn.2466. PubMed PMID: 20037578; PubMed Central PMCID: PMC3634157.
37. Schuz A, Palm G. Density of neurons and synapses in the cerebral cortex of the mouse. J Comp Neurol. 1989;286(4):442-55. doi: 10.1002/cne.902860404. PubMed PMID: 2778101.
38. Bakin JS, Weinberger NM. Classical conditioning induces CS-specific receptive field plasticity in the auditory cortex of the guinea pig. Brain Res. 1990;536(1-2):271-86. Epub 1990/12/17. PubMed PMID: 2085753.
39. Recanzone GH, Schreiner CE, Merzenich MM. Plasticity in the frequency representation of primary auditory cortex following discrimination training in adult owl monkeys. J Neurosci. 1993;13(1):87-103. PubMed PMID: 8423485.
40. Harper NS, McAlpine D. Optimal neural population coding of an auditory spatial cue. Nature. 2004;430(7000):682-6. doi: 10.1038/nature02768. PubMed PMID: 15295602.
41. Dean I, Harper NS, McAlpine D. Neural population coding of sound level adapts to stimulus statistics. Nat Neurosci. 2005;8(12):1684-9. doi: 10.1038/nn1541. PubMed PMID: 16286934.
42. Han YK, Kover H, Insanally MN, Semerdjian JH, Bao S. Early experience impairs perceptual discrimination. Nat Neurosci. 2007;10(9):1191-7. doi: 10.1038/nn1941. PubMed PMID: 17660815.
43. Whitton JP, Hancock KE, Polley DB. Immersive audiomotor game play enhances neural and perceptual salience of weak signals in noise. Proc Natl Acad Sci U S A. 2014;111(25):E2606-15. doi: 10.1073/pnas.1322184111. PubMed PMID: 24927596; PubMed Central PMCID: PMCPMC4078866.
44. Ahrens M, Linden J, Sahani M. Nonlinearities and contextual influences in auditory cortical responses modeled with multilinear spectrotemporal methods. J Neurosci. 2008;28(8):1929-42. doi: 10.1523/JNEUROSCI.3377-07.2008. PubMed PMID: 18287509.
45. Carruthers IM, Natan RG, Geffen MN. Encoding of ultrasonic vocalizations in the auditory cortex. J Neurophysiol. 2013;109(7):1912-27. Epub 2013/01/18. doi: 10.1152/jn.00483.2012. PubMed PMID: 23324323.
46. Hermundstad AM, Briguglio JJ, Conte MM, Victor JD, Balasubramanian V, Tkacik G. Variance predicts salience in central sensory processing. Elife. 2014;3. doi: 10.7554/eLife.03722. PubMed PMID: 25396297; PubMed Central PMCID: PMCPMC4271187.
47. Tkacik G, Prentice JS, Victor JD, Balasubramanian V. Local statistics in natural scenes predict the saliency of synthetic textures. Proc Natl Acad Sci U S A. 2010;107(42):18149-54. doi: 10.1073/pnas.0914916107. PubMed PMID: 20923876; PubMed Central PMCID: PMCPMC2964243.
48. Geffen MN, Gervain J, Werker JF, Magnasco MO. Auditory perception of self-similarity in water sounds. Front Integr Neurosci. 2011;5:15. doi: 10.3389/fnint.2011.00015. PubMed PMID: 21617734; PubMed Central PMCID: PMC3095814.
49. Gervain J, Werker JF, Geffen MN. Category-specific processing of scale-invariant sounds in infancy. PLoS One. 2014;9(5):e96278. doi: 10.1371/journal.pone.0096278. PubMed PMID: 24809801; PubMed Central PMCID: PMC4014493.

755 50. Gervain J, Werker JF, Black A, Geffen MN. The neural correlates of processing scale-invariant
756 environmental sounds at birth. Neuroimage. 2016;133:144-50. doi: 10.1016/j.neuroimage.2016.03.001.
757 PubMed PMID: 26956907.
758 51. Chow BY, Han X, Dobry AS, Qian X, Chuong AS, Li M, et al. High-performance genetically targetable
759 optical neural silencing by light-driven proton pumps. Nature. 2010;463(7277):98-102. Epub 2010/01/08.
760 doi: 10.1038/nature08652. PubMed PMID: 20054397; PubMed Central PMCID: PMC2939492.
761 52. Atasoy D, Aponte Y, Su HH, Sternson SM. A FLEX switch targets Channelrhodopsin-2 to multiple
762 cell types for imaging and long-range circuit mapping. J Neurosci. 2008;28(28):7025-30. Epub 2008/07/11.
763 doi: 10.1523/JNEUROSCI.1954-08.2008. PubMed PMID: 18614669; PubMed Central PMCID: PMC2593125.
764 53. Clause A, Nguyen T, Kandler K. An acoustic startle-based method of assessing frequency
765 discrimination in mice. J Neurosci Methods. 2011;200(1):63-7. doi: 10.1016/j.jneumeth.2011.05.027.
766 54. Mwilambwe-Tshilobo L, Davis AJ, Aizenberg M, Geffen MN. Selective Impairment in Frequency
767 Discrimination in a Mouse Model of Tinnitus. PLoS One. 2015;10(9):e0137749. Epub 2015/09/10. doi:
768 10.1371/journal.pone.0137749. PubMed PMID: 26352864; PubMed Central PMCID: PMC4564173.
769